Comparative Performance of ^{18}F-FDG PET/MRI and ^{18}F-FDG PET/CT in Detection and Characterization of Pulmonary Lesions in 121 Oncologic Patients

Lino M. Sawicki[1,2], Johannes Grueneisen[2], Christian Buchbender[1], Benedikt M. Schaarschmidt[1], Benedikt Gomez[3], Verena Ruhlmann[3], Axel Wetter[2], Lale Umutlu[2], Gerald Antoch[1], and Philipp Heusch[1]

[1]Department of Diagnostic and Interventional Radiology, University Dusseldorf, Dusseldorf, Germany; [2]Department of Diagnostic and Interventional Radiology and Neuroradiology, University Duisburg-Essen, Essen, Germany; and [3]Department of Nuclear Medicine, University Duisburg-Essen, Essen, Germany

Our objective was to compare ^{18}F-FDG PET/MRI (performed using a contrast-enhanced T1-weighted fat-suppressed volume-interpolated breath-hold examination [VIBE]) with ^{18}F-FDG PET/CT for detecting and characterizing lung lesions in oncologic patients. **Methods:** In 121 oncologic patients with 241 lung lesions, PET/MRI was performed after PET/CT in a single-injection protocol (260 ± 58 MBq of ^{18}F-FDG). The detection rates were computed for MRI, the PET component of PET/CT, and the PET component of PET/MRI in relation to the CT component of PET/CT. Wilcoxon testing was used to assess differences in lesion contrast (4-point scale) and size between morphologic datasets and differences in image quality (4-point scale), SUV_{mean}, SUV_{max}, and characterization (benign/malignant) between PET/MRI and PET/CT. Correlation was determined using the Pearson coefficient (r) for SUV and size and the Spearman rank coefficient (ρ) for contrast. **Results:** The detection rates for MRI, the PET component of PET/CT, and the PET component of PET/MRI were 66.8%, 42.7%, and 42.3%, respectively. There was a strong correlation in size ($r = 0.98$) and SUV ($r = 0.91$) and a moderate correlation in contrast ($\rho = 0.48$). Image quality was better for PET/CT than for PET/MRI ($P < 0.001$). Lesion measurements were smaller for MRI than for CT ($P < 0.001$). SUV_{max} and SUV_{mean} were significantly higher for PET/MRI than for PET/CT ($P < 0.001$ each). There was no significant difference in lesion contrast ($P = 0.11$) or characterization ($P = 0.076$). **Conclusion:** In the detection and characterization of lung lesions 10 mm or larger, ^{18}F-FDG PET/MRI and ^{18}F-FDG PET/CT perform comparably. Lesion size, SUV and characterization correlate strongly between the two modalities. However, the overall detection rate of PET/MRI remains inferior to that of PET/CT because of the limited ability of MRI to detect lesions smaller than 10 mm. Thus, thoracic staging with PET/MRI bears a risk of missing small lung metastases.

Key Words: lung; lesion; MRI; PET/MRI; PET/CT

J Nucl Med 2016; 57:582–586
DOI: 10.2967/jnumed.115.167486

Pulmonary lesion detection and characterization play a key role in cancer staging, as the presence of lung metastases influences therapy regimens and patient survival (*1–3*). CT, offering high spatial resolution of pulmonary tissue, has been regarded as the reference standard for lung lesion detection (*4,5*). However, because morphologic CT-based criteria have a relatively low specificity for malignant versus benign character, there has been a need for a more robust diagnostic standard. Over the last decade, ^{18}F-FDG PET/CT has proven successful not only in detecting pulmonary lesions but also in discriminating benign from malignant findings, taking advantage of the accurate anatomic information from CT and the functional characterization from PET in a one-stop-shop examination (*6–8*). Yet, a major drawback of ^{18}F-FDG PET/CT is the low sensitivity of the PET component in pulmonary lesions smaller than 10 mm, because of motion artifacts, partial-volume effects, and the limited spatial resolution of PET (*9*). MRI has played only a minor role in radiologic assessment of the lung, mainly because of methodologic and physical shortcomings such as low proton density in aerated lungs, fast decay of signal, and motion artifacts caused by breathing and cardiac pulsation. When different MRI sequences are compared, it is the T1-weighted 3-dimensional (3D) gradient echo sequences—such as T1-weighted volume-interpolated breath-hold examination (VIBE)—that demonstrate the highest sensitivity and thus are recommended for MR-based identification of pulmonary lesions (*3–5*). Nevertheless, several studies have indicated that lesion detection on MRI remains inferior to that on CT (*4,10,11*). The recently introduced fully integrated whole-body PET/MRI combines simultaneously acquired metabolic information from PET with high soft-tissue contrast and functional information from MRI to allow for improved assessment of tumor burden in cancer patients (*12–14*). In view of the challenges of MRI in pulmonary imaging, the increasing use of whole-body PET/MRI has sparked interest in determining its performance in depicting lung lesions. Not only is the comparison of morphologic imaging datasets (MRI vs. CT) of great interest but also the comparison of PET from PET/MRI versus PET from PET/CT, considering the differences in PET acquisition and attenuation correction techniques between the two. Existing evidence in this field is based on one study by Chandarana et al. and another by Rauscher et al., the former with 32 patients and the latter with 40 (*15,16*).

Thus, the purpose of our study was to compare ^{18}F-FDG PET/MRI (performed using contrast-enhanced T1-weighted fat-suppressed VIBE) with ^{18}F-FDG PET/CT for detecting and characterizing lung lesions in a large cohort of oncologic patients.

Received Sep. 30, 2015; revision accepted Nov. 16, 2015.
For correspondence or reprints contact: Lino M. Sawicki, University Dusseldorf, Medical Faculty, Department of Diagnostic and Interventional Radiology, D-40225 Dusseldorf, Germany.
E-mail: linomorris.sawicki@med.uni-duesseldorf.de
Published online Jan. 7, 2016.

MATERIALS AND METHODS

Patients and Inclusion Criteria

This study included all patients with proven or suspected malignancies (Table 1) who, between May 2012 and December 2014, underwent ^{18}F-FDG PET/MRI (including a contrast-enhanced T1-weighted fat-suppressed VIBE sequence of the thorax) after a clinically scheduled staging ^{18}F-FDG PET/CT study on the same day. In total, 121 subjects (mean age ± SD, 57.1 ± 13.9 y; 71 women and 50 men) were eligible for retrospective analysis. The study was approved by the local ethics committee, and all subjects signed an informed consent form.

PET/CT

Whole-body PET/CT was performed on a Biograph mCT or Biograph Duo scanner (Siemens Healthcare GmbH) 61 ± 10.3 min after intravenous injection of 260 ± 58 MBq of ^{18}F-FDG, depending on patient body weight. Blood glucose levels were verified to be below 150 mg/dL at injection time. Patients were examined using full-dose (n = 67) or low-dose (n = 54) technique. For full-dose scans, an iodinated contrast medium was administered (Imeron 300; Bracco Imaging Deutschland GmbH) and a dedicated low-dose lung scan applying a sharp B70 or B90 kernel in deep inspiration was additionally acquired. All CT images were displayed using a transverse lung window setting with a slice thickness of 2 mm. Manufacturer-supplied dose reduction software (CareKV and CareDose 4D) was available for both full-dose and low-dose PET/CT scans using presets of 120 kV, 210 mAs, and 120 kV, 40 mAs, respectively. The PET acquisition time using static frames varied from 2 to 3.5 min per bed position, with an average of 7 bed positions needed to cover the body volume. Iterative reconstruction (3 iterations and 21 subsets) and a gaussian filter of 4 mm were applied. In general, PET images were reconstructed with a slice thickness of 3 mm. The portal venous phase of full-dose CT scans and the low-dose CT data of low-dose CT scans were used for attenuation correction of the PET images.

PET/MRI

Whole-body ^{18}F-FDG PET/MRI using flex coils was performed on a 3-T Biograph mMR scanner (Siemens Healthcare GmbH). PET/MRI scans began with the shortest possible delay after PET/CT (113.9 ± 28.5 min after radiotracer injection). First, a coronal 3D Dixon VIBE sequence (repetition time, 3.6 ms; first echo time, 1.23 ms; second echo time, 2.46 ms; slice thickness, 3.12 mm; field of view, 500 × 328 mm; matrix size, 192 × 121; voxel size, 4.1 × 2.6 × 3.1 mm) was acquired to generate a map for MR-based attenuation correction. Then, personalized MRI protocols were performed, depending on each patient's clinical implications. The only morphologic dataset for lung assessment in this study was a transverse T1-weighted fat-suppressed VIBE MRI sequence (repetition time, 4.08 ms; echo time, 1.51 ms; slice thickness, 3.5 mm; field of view, 400 × 300 mm; matrix size, 512 × 307.2; voxel size, 1.3 × 0.8 × 3.5 mm) performed after administration of a gadolinium-based contrast medium (Dotarem; Guerbet GmbH). This dataset was used for PET/MR image fusion. For imaging of the thorax, the MRI sequence was acquired during breath-hold in deep inspiration. Acquisition speed was increased through application of generalized, autocalibrating, partially parallel acquisitions with an acceleration factor of 2. In general, the PET acquisition time was 3 min per bed position (2 bed positions for the whole thorax) starting simultaneously with acquisition of the 3D Dixon VIBE sequence. PET images were acquired in list mode and reconstructed in the same way as for PET/CT, using ordered-subsets expectation maximization with 3 iterations and 21 subsets, a gaussian filter of 4 mm, and a slice thickness of 3 mm.

TABLE 1
Tumor Types in Study Cohort

Type	*n*
Lung cancer	28
Lymphoma	21
Breast cancer	18
Uterine cancer	12
Ovarian cancer	10
Cancer of unknown primary	8
Malignant melanoma	4
Head and neck cancer	4
Gastrointestinal cancer	3
Malignant mesothelioma	3
Other (<3 cases/type)	10

Image Analysis

All imaging datasets were evaluated on an OsiriX workstation (Pixmeo SARL) and independently analyzed by 2 radiologists with 3 and 4 y of experience in PET/CT and PET/MRI interpretation. Any discrepancies between the interpreters were resolved in a subsequent consensus interpretation. The interpreters did not know the patients' history. PET/CT and PET/MRI were assessed in separate sessions and in random order a minimum of 4 wk apart to avoid recognition bias. Morphologic chest images (MRI and CT), as well as PET from PET/CT and PET from PET/MRI, were analyzed separately and as fused PET/CT and PET/MRI datasets. PET images were reviewed with and without attenuation correction to prevent false-positive findings caused by attenuation-correction artifacts. The interpreters evaluated the quality of each fused PET/CT and PET/MRI image using a 4-point scale (1 = very poor image quality: major artifacts, no diagnostic value; 2 = poor image quality: distinct artifacts, considerably limited diagnostic use; 3 = good image quality: minor artifacts, marginally limited diagnostic use; 4 = excellent image quality: no artifacts, unconditional diagnostic use). As previously described by Rauscher et al. (*16*), CT and PET from PET/CT as well as MRI and PET from PET/MRI were assessed separately with regard to the presence and number of lesions, with the CT component of PET/CT serving as the standard of reference. A maximum of 10 lesions was identified for each patient, starting from the right upper lobe and proceeding to the left lower lobe. Lesion size (longitudinal axis diameter) in millimeters was measured on MRI and CT. Lesion contrast on MRI and CT was qualitatively assessed using a 4-point scale (1 = very low contrast; 2 = low contrast; 3 = moderate contrast; 4 = high contrast). The presence of focal tracer uptake above the surrounding background level (morphologically unaltered lung tissue) was noted for each lesion. For quantitative assessment and comparison of tracer uptake, SUV_{mean} and SUV_{max} were evaluated by placing a freehand polygonal volume of interest over each lesion on the corresponding attenuation-corrected PET image from PET/CT and PET/MRI. OsiriX software automatically calculated SUV_{mean} and SUV_{max} from the volumes of interest on the PET images. Each lesion was rated for its presumed character (1 = most likely benign; 2 = indeterminate; 3 = suggestive of malignancy) on the basis of the presence of a focus of ^{18}F-FDG uptake and typical morphologic criteria for benign and malignant pulmonary nodules as established by Seemann et al. (*17,18*).

Statistics

SPSS Statistics, version 22 (IBM), was used for statistical analysis. All data are given as mean ± SD. A P value of less than 0.05 was considered to be statistically significant. Data were tested for normal

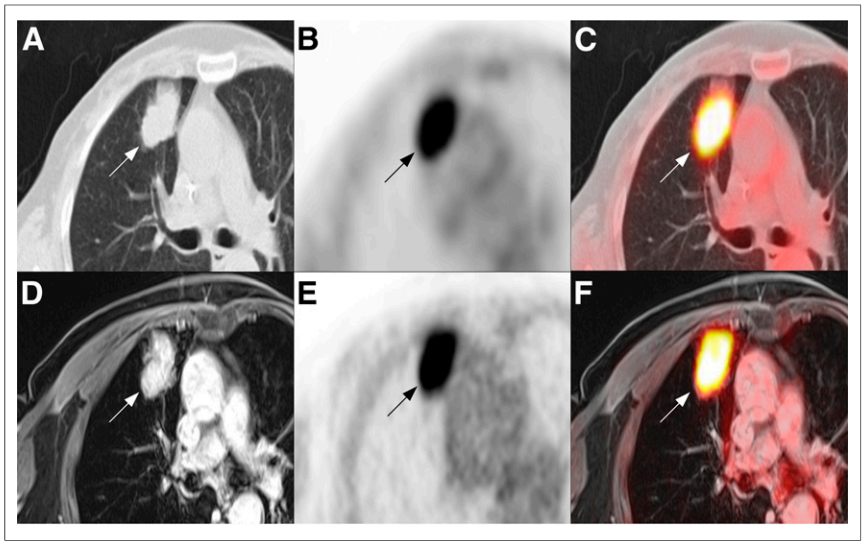

FIGURE 1. In 65-y-old woman with lung cancer, 38-mm tumor (arrows) is seen in right upper lobe of lung on CT component (A) of PET/CT (C) and on MRI component (D) of PET/MRI (F). SUV_{max} of strong ^{18}F-FDG uptake on PET component is 17.3 for PET/CT (B) and 19.4 for PET/MRI (E).

distribution using the Kolmogorov–Smirnov test. Descriptive analysis was performed. Wilcoxon tests were used to evaluate differences in SUV_{mean}, SUV_{max}, size, image quality, lesion contrast, and lesion characterization. Correlation between PET/MRI and PET/CT was assessed using the Pearson coefficient (r) for SUV_{mean}, SUV_{max}, and size and the Spearman rank coefficient (ρ) for lesion contrast and lesion characterization. Detection rates were calculated by dividing the respective total number of lesions detected on MRI, PET from PET/CT, and PET from PET/MRI by the total number of lesions found on the CT component of PET/CT as the reference standard.

RESULTS

Lesion Detection

According to the standard of reference, 241 lesions measuring 13.1 ± 15.2 mm (range, 1–98 mm) were found in 84 of 121 patients. MRI showed an overall detection rate of 66.8%. The detection rates of MRI for lesions smaller than 10 mm, smaller than 5 mm, and 10 mm or larger were 45.9%, 43.1%, and 94.9%, respectively. A separate evaluation of MRI detection rates with respect to either low-dose lung scans performed in deep inspiration as part of the full-dose PET/CT protocol or low-dose lung scans performed in shallow breathing from low-dose PET/CT yielded detection rates of 62.1% and 72.5%, respectively, suggesting that more lesions were missed on MRI as compared with CT performed in deep inspiration. However, the Mann–Whitney U test showed that the average number of missed lesions on MRI versus CT in deep inspiration (0.75 ± 1.11) and CT in shallow breathing (0.56 ± 1.25) did not differ significantly ($P = 0.146$). The resolution limits for lesions were 1 mm on CT and 3 mm on MRI. The PET components of PET/CT and of PET/MRI demonstrated focal tracer uptake in 42.7% and 42.3% of all lesions, respectively. There was no focal uptake on PET images from PET/MRI or PET/CT that did not correspond to a visual morphologic correlate on MRI or CT, respectively. Hence, the detection rate of fused PET/MRI and PET/CT was identical to that of its respective morphologic imaging component. Figures 1 and 2 show different examples of lesions on PET/CT and PET/MRI.

Comparison of Lesion Size and Lesion Contrast

Analysis of lesion size revealed that corresponding lesions detected on both MRI and CT ($n = 161$) measured significantly smaller ($P < 0.001$) on MRI (average size, 17.1 ± 16.8 mm) than on CT (17.7 ± 16.9 mm). The smaller size of corresponding lesions on MRI was a constant phenomenon; thus, there was a strong correlation in lesion size between the two modalities ($r = 0.98$; $P < 0.001$). Figure 3 shows a linear regression analysis and a Bland–Altman plot. The average contrast for corresponding lesions was high on CT (3.65 ± 0.6) and MRI (3.61 ± 0.7), with no significant difference between the modalities ($P = 0.11$). Contrast for corresponding lesions showed a moderate positive correlation between CT and MRI ($\rho = 0.48$; $P < 0.001$).

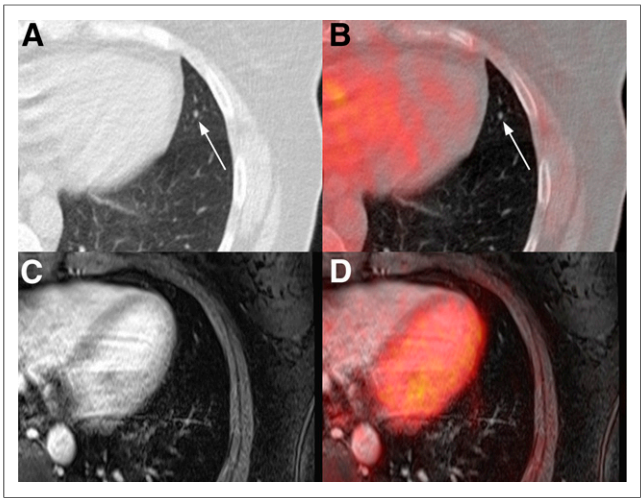

FIGURE 2. In 46-y-old woman with breast cancer, 4-mm nodule (arrows) is seen in lingula segment of left upper lobe of lung on CT component (A) of PET/CT (B) but not on MRI component (C) of PET/MRI (D). No ^{18}F-FDG uptake is seen on PET component of either PET/CT (C) or PET/MRI (D).

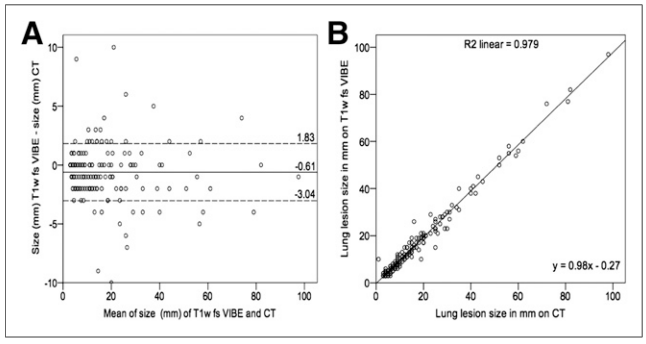

FIGURE 3. (A) For each of 161 lung lesions, difference between size on MRI component of PET/MRI and size on CT component of PET/CT is plotted against mean size, which was −0.61 mm (95% confidence interval, 1.83 and −3.04 mm). (B) Linear regression plot demonstrates correlation between size on MRI and size on CT ($r = 0.98$; $P < 0.001$). T1w fs = T1-weighted fat saturation.

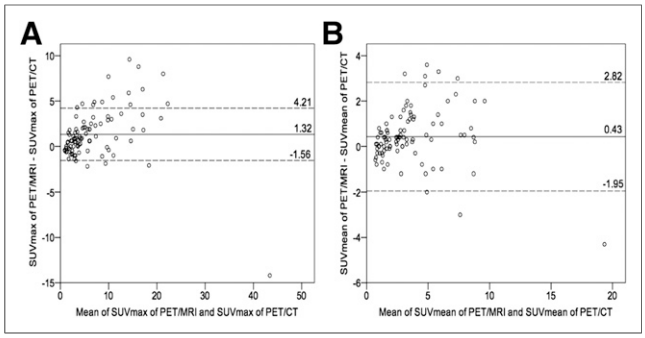

FIGURE 4. (A) For each of 161 lung lesions, difference in SUV_{max} (A) and SUV_{mean} (B) between PET component of PET/MRI and PET component of PET/CT is plotted against mean difference, which was 1.32 for SUV_{max} (95% confidence interval, 4.21 and −1.56) and 0.43 for SUV_{mean} (95% confidence interval, 2.82 and −1.95).

Quantitative Assessment of SUV

For 96 corresponding PET-positive lesions detected on both modalities, the average SUV_{max} and SUV_{mean} were significantly higher for PET/MRI than PET/CT (respectively, 7.39 ± 6.7 vs. 6.09 ± 6.5 for SUV_{max} and 3.73 ± 2.9 vs. 3.3 ± 2.9 for SUV_{mean}; $P < 0.001$ each). A strong positive correlation was found for SUV_{max} ($r = 0.91$; $P < 0.001$) and SUV_{mean} ($r = 0.91$; $P < 0.001$) between the two hybrid imaging modalities. A Bland–Altman plot illustrating differences in SUV measurements between PET/CT and PET/MRI can be found in Figure 4.

Lesion Characterization

On both modalities, most lesions were characterized as either most likely benign or suggestive of malignancy, whereas only a small proportion was characterized as indeterminate. Because the number of lesions detected with PET/MRI was smaller than the number detected with PET/CT, and MRI detected mainly larger lesions, a greater proportion of lesions was characterized as suggestive of malignancy with PET/MRI than with PET/CT (66% vs. 41%). The characterization of the 161 corresponding lesions that were found both on PET/CT and on PET/MRI did not significantly differ ($P = 0.076$) and correlated strongly ($\rho = 0.87$; $P < 0.001$) (Table 2).

Image Quality

The mean image quality for both PET/MRI and PET/CT was rated as good to excellent. However, the Wilcoxon test yielded a significantly lower mean image quality for PET/MRI than for PET/CT (3.5 ± 0.5 vs. 3.7 ± 0.5; $P < 0.001$).

DISCUSSION

The results of our study indicate that the detection rates of ^{18}F-FDG PET/MRI and ^{18}F-FDG PET/CT are nearly equivalent for pulmonary lesions 10 mm or larger. However, the detectability of lung lesions smaller than 10 mm on PET/MRI remained inferior with the currently recommended T1-weighted 3D volume-interpolated gradient echo MRI sequence as the morphologic dataset. The PET datasets from PET/MRI and PET/CT delivered comparable results.

Considering the nearly equivalent performance of both hybrid imaging modalities for lesions 10 mm or larger and that characterization did not vary significantly, our study seems to support the general applicability of PET/MRI as an alternative to PET/CT in the staging of tumors that have metastasized to the lung. The applicability of PET/MRI is substantiated by the fact that both hybrid imaging modalities showed good to excellent image quality and the fact that corresponding lesion contrast was similar. However, as MRI missed more than half the pulmonary lesions smaller than 10 mm, the overall diagnostic performance of the MRI component of PET/MRI was still outmatched by the CT component of PET/CT. Because only one third of the lung consists of tissue and two thirds air, proton density is substantially lower in the lung than in any other human organ. Rapid signal loss and motion artifacts from cardiac or aortic pulsation and breathing additionally impair the signal-to-noise ratio in MRI. By effectively exploiting the signal from available protons, T1-weighted gradient echo sequences (e.g., VIBE) with a short echo time (<7 ms) have proven superior to a longer echo time or to spin echo or pulse sequences for depicting lung lesions and are thus recommended for MR-based lesion detection (*19*). The reasons for the inferiority of PET/MRI are found in the methodologic shortcomings of MRI at depicting small lung nodules, which accounted for most lesions in our study. Studies by Sommer et al., Biederer et al., and Müller et al. evaluating CT and MRI corroborate these findings (*4,10,11*). Moreover, two recently published studies by Chandarana et al. and Rauscher et al. comparing ^{18}F-FDG PET/MRI and ^{18}F-FDG PET/CT yielded similar detection rates of 68% and 70% for T1-weighted VIBE images compared with diagnostic CT (*15,16*). The clinical impact of this finding, however, remains controversial as most small pulmonary nodules are known to be noncancerous even in patients with a proven malignancy (*20*). Nevertheless, the presence of early-stage lung metastases cannot be excluded and the risk of missing metastatic spread has to be considered when solely PET/MRI is performed. Thus, further development toward more sensitive MR sequences seems required in order for PET/MRI to be accepted as an independent staging modality. In patients with proven or suspected malignancy, ^{18}F-FDG–avid lung lesions are generally considered suggestive of malignancy. As a result of the nearly equivalent performance of both PET components and the lower number of small lesions identified on MRI, a greater proportion of lesions would be expected to be rated malignant on PET/MRI than on PET/CT. This expectation was substantiated by our study, in which 25% more lesions were suggestive of malignancy on PET/MRI than on PET/CT.

In concordance with prior studies, our study found a strong positive correlation between SUV measurements (*15,16,21*). Additionally, we

TABLE 2
Lung Lesion Characterization on PET/CT and PET/MRI

Modality	Lesions detected (*n*)			
	Total	Most likely benign	Indeterminate	Suggestive of malignancy
PET/CT	241	110 (46%)	31 (13%)	100 (41%)
PET/MRI	161	41 (25%)	14 (9%)	106 (66%)

confirmed the propensity for slightly higher SUVs on PET/MRI than on PET/CT (*15,16,22,23*). The underlying reasons are not yet completely understood, but it is assumed that in addition to differences in scanner technology, biologic factors may play a role. Because patients underwent PET/CT first, the interval between imaging and radiotracer injection was longer for PET/MRI than for PET/CT (114 min vs. 61 min). Tissues with a high glucose turnover such as lung metastases are hypothesized to have an increased level of intracellular tracer trapping on delayed time-point images (*24,25*).

Although we found a strong positive correlation in size measurements, there was a significant tendency for corresponding pulmonary lesions to measure smaller on PET/MRI than on PET/CT. Again, this finding is probably due to technical differences between the two morphologic datasets. Although the higher spatial resolution of CT allows for precise lesion depiction, the fast decay of MR signal at air–tissue interfaces compromises detailed imaging at the periphery of a lesion (*19*).

Our study had some limitations. First, we did not evaluate other MR sequences, such as T2-weighted single-shot turbo spin echo or radial blade. Although a multisequence MR protocol might arguably increase the detection rate of PET/MRI, any improvement would probably be marginal because T1-weighted 3D volume-interpolated gradient echo sequences offer the highest sensitivity, especially in small pulmonary lesions, whereas T2-weighted sequences are adequate for visualizing infiltrates or adjacent mediastinum (*26*). A second limitation was that the use of two different PET/CT protocols (one with low-dose chest CT in deep inspiration and one without) may have underestimated the total number of lung nodules on the reference standard. However, our data suggest that deep-inspiration acquisition has no significant advantage over shallow-breathing acquisition in identifying missed lesions on lung PET/CT.

CONCLUSION

Our study has shown that ^{18}F-FDG PET/MRI of the thorax has high image quality and detection rates similar to ^{18}F-FDG PET/CT for pulmonary lesions 10 mm or larger, thus supporting its general applicability as an alternative to PET/CT in the staging of oncologic patients. Notwithstanding technical differences, the detection rates of the PET datasets from both hybrid imaging modalities are comparable. Furthermore, there is a strong positive correlation between PET/MRI and PET/CT in the size, SUV_{max}, SUV_{mean}, and characterization of lesions. However, the overall detection rate of PET/MRI remains inferior to that of PET/CT because of the lower detectability of pulmonary lesions smaller than 10 mm on T1-weighted 3D volume-interpolated gradient echo sequences. Hence, tumor staging with PET/MRI bears a risk of missing small lung metastases. Thus, further research on more sensitive MR sequences seems required.

DISCLOSURE

The costs of publication of this article were defrayed in part by the payment of page charges. Therefore, and solely to indicate this fact, this article is hereby marked "advertisement" in accordance with 18 USC section 1734. No potential conflict of interest relevant to this article was reported.

REFERENCES

1. Edge SB, Byrd DR, Compton CC, Fritz AG, Greene FL, Trotti A. *AJCC Cancer Staging Manual.* 7th ed. New York, NY: Springer; 2010.
2. Barth A, Wanek LA, Morton DL. Prognostic factors in 1,521 melanoma patients with distant metastases. *J Am Coll Surg.* 1995;181:193–201.
3. Biederer J, Beer M, Hirsch W, et al. MRI of the lung (2/3). Why ... when ... how? *Insights Imaging.* 2012;3:355–371.
4. Sommer G, Koenigkam-Santos M, Biederer J, Puderbach M. Role of MRI for detection and characterization of pulmonary nodules. *Radiologe.* 2014;54:470–477.
5. Biederer J, Hintze C, Fabel M. MRI of pulmonary nodules: technique and diagnostic value. *Cancer Imaging.* 2008;8:125–130.
6. Cistaro A, Lopci E, Gastaldo L, Fania P, Brach Del Prever A, Fagioli F. The role of ^{18}F-FDG PET/CT in the metabolic characterization of lung nodules in pediatric patients with bone sarcoma. *Pediatr Blood Cancer.* 2012;59:1206–1210.
7. Dabrowska M, Krenke R, Korczynski P, et al. Diagnostic accuracy of contrast-enhanced computed tomography and positron emission tomography with 18-FDG in identifying malignant solitary pulmonary nodules. *Medicine (Baltimore).* 2015;94:e666.
8. Opoka L, Kunikowska J, Podgajny Z, et al. Accuracy of FDG PET/CT in the evaluation of solitary pulmonary lesions: own experience. *Pneumonol Alergol Pol.* 2014;82:198–205.
9. Tan BB, Flaherty KR, Kazerooni EA, Iannettoni MD. The solitary pulmonary nodule. *Chest.* 2003;123(suppl):89S–96S.
10. Biederer J, Schoene A, Freitag S, Reuter M, Heller M. Simulated pulmonary nodules implanted in a dedicated porcine chest phantom: sensitivity of MR imaging for detection. *Radiology.* 2003;227:475–483.
11. Müller NL, Gamsu G, Webb WR. Pulmonary nodules: detection using magnetic resonance and computed tomography. *Radiology.* 1985;155:687–690.
12. Drzezga A, Souvatzoglou M, Eiber M, et al. First clinical experience with integrated whole-body PET/MR: comparison to PET/CT in patients with oncologic diagnoses. *J Nucl Med.* 2012;53:845–855.
13. Buchbender C, Heusner TA, Lauenstein TC, Bockisch A, Antoch G. Oncologic PET/MRI, part 1: tumors of the brain, head and neck, chest, abdomen, and pelvis. *J Nucl Med.* 2012;53:928–938.
14. Buchbender C, Heusner TA, Lauenstein TC, Bockisch A, Antoch G. Oncologic PET/MRI, part 2: bone tumors, soft-tissue tumors, melanoma, and lymphoma. *J Nucl Med.* 2012;53:1244–1252.
15. Chandarana H, Heacock L, Rakheja R, et al. Pulmonary nodules in patients with primary malignancy: comparison of hybrid PET/MR and PET/CT imaging. *Radiology.* 2013;268:874–881.
16. Rauscher I, Eiber M, Furst S, et al. PET/MR imaging in the detection and characterization of pulmonary lesions: technical and diagnostic evaluation in comparison to PET/CT. *J Nucl Med.* 2014;55:724–729.
17. Seemann MD, Seemann O, Luboldt W, et al. Differentiation of malignant from benign solitary pulmonary lesions using chest radiography, spiral CT and HRCT. *Lung Cancer.* 2000;29:105–124.
18. Seemann MD, Staebler A, Beinert T, et al. Usefulness of morphological characteristics for the differentiation of benign from malignant solitary pulmonary lesions using HRCT. *Eur Radiol.* 1999;9:409–417.
19. Kauczor HU, Kreitner KF. Contrast-enhanced MRI of the lung. *Eur J Radiol.* 2000;34:196–207.
20. Benjamin MS, Drucker EA, McLoud TC, Shepard JA. Small pulmonary nodules: detection at chest CT and outcome. *Radiology.* 2003;226:489–493.
21. Heusch P, Buchbender C, Kohler J, et al. Thoracic staging in lung cancer: prospective comparison of ^{18}F-FDG PET/MR imaging and ^{18}F-FDG PET/CT. *J Nucl Med.* 2014;55:373–378.
22. Pace L, Nicolai E, Luongo A, et al. Comparison of whole-body PET/CT and PET/MRI in breast cancer patients: lesion detection and quantitation of ^{18}F-deoxyglucose uptake in lesions and in normal organ tissues. *Eur J Radiol.* 2014; 83:289–296.
23. Paspulati RM, Partovi S, Herrmann KA, Krishnamurthi S, Delaney CP, Nguyen NC. Comparison of hybrid FDG PET/MRI compared with PET/CT in colorectal cancer staging and restaging: a pilot study. *Abdom Imaging.* 2015;40:1415–1425.
24. Cheng G, Torigian DA, Zhuang H, Alavi A. When should we recommend use of dual time-point and delayed time-point imaging techniques in FDG PET? *Eur J Nucl Med Mol Imaging.* 2013;40:779–787.
25. Costantini DL, Vali R, Chan J, McQuattie S, Charron M. Dual-time-point FDG PET/CT for the evaluation of pediatric tumors. *AJR.* 2013;200:408–413.
26. Fink C, Puderbach M, Biederer J, et al. Lung MRI at 1.5 and 3 Tesla: observer preference study and lesion contrast using five different pulse sequences. *Invest Radiol.* 2007;42:377–383.